ELSEVIER

Journal of Nuclear Materials 255 (1998) 128–138

journal of nuclear materials

Low-activation Mn–Cr austenitic stainless steel with further reduced content of long-lived radioactive elements

Masanori Onozuka [a,*], Tomikane Saida [a], Shouzou Hirai [a], Mikio Kusuhashi [b], Ikuo Sato [b], Tsuyoshi Hatakeyama [b]

[a] *Mitsubishi Heavy Industries Ltd., Minatomirai, 3-3-1, Nishi-ku, Yokohama 220-8401, Japan*
[b] *The Japan Steel Works Ltd., Chatsu-machi 4, Muroran 051-8505, Japan*

Received 29 August 1997; accepted 7 February 1998

Abstract

Low-activation austenitic stainless steel based on Mn–Cr non-magnetic steels has been developed. The alloying elements of long-life activation, such as Ni, Mo and Co, were eliminated and substituted with Mn along with an addition of N. A Mn–Cr austenitic stainless steel, 24.5Mn–13.5Cr–0.02C–0.2N, has been developed successfully. Examined material properties, including mechanical, thermal and magnetic properties, as well as weldability and characteristics of corrosion resistance, are presented. It was found that the alloy has excellent material properties virtually equivalent to those of 316SS. In this study, the applicability of the Schaeffler, DeLong and Hull constitution diagrams for the stainless steels with low Ni and high Mn contents was also examined. The boundary conditions distinguishing the single austenite phase from the others have been identified for the Mn–Cr steels.

PACS: 28.52.Fa: Materials; 28.52.-S: Fusion reactors

1. Introduction

Long-lived radioactivity of components after irradiation is a concern of fusion reactors regarding safety, recycling and waste disposal [1,2]. In order to reduce the level of radioactivity, vigorous efforts have been made to develop low activation austenitic stainless steels by substituting Mn, C, V, etc., which have an equivalent influence on the alloy constitution but a lower radiological impact, for long-life activation elements, such as Ni, Mo, Nb and Co in commercially produced steels [3–8]. Various types of low activation austenitic stainless steels have been investigated based on Mn–Cr non-magnetic steels [4–8]. Mn–Cr steels generally have comparable unirradiated mechanical properties with type 316 stainless steel (316SS). However, it has been reported that the phase and properties of Mn–Cr steels are unstable under irradiation at high temperature (such as conditions higher than 450°C and 70 dpa) [9,10]. Although the applicability of the steels to fusion reactor components may be limited due to such characteristics, further investigation has being conducted to optimize their properties and minimize the effects of radiation damage [11–13].

Piatti et al. [4,6], Piatti and Schiller [5], Zucchetti and Zublena [7], Merola and Zucchetti [8], and Shamardin et al. [11,12] have investigated various types of low activation austenitic stainless steel based on Mn–Cr non-magnetic steels. However, those alloys still have small amounts of Ni, Mo, etc. that cause problems of long-life activation [2]. In the present study, research has been conducted to eliminate such undesirable elements and produce lower activation austenitic stainless steels that can be manufactured along usual industrial production lines.

* Corresponding author. Present address: ITER Garching Joint Work Site, c/o Max-Planck-Institut für Plasmaphysik, Boltzmannstraße 2, D-85748 Garching bei München, Germany. Tel.: +49-89 3299 4152; fax: +49-89 3299 4422; e-mail: onozukm@sat.ipp-garching.mpg.de.

0022-3115/98/$19.00
PII: S0022-3115(98)00031-2

2. Development of low-activation austenitic stainless steel

2.1. Adjustment of alloying elements

Adjustment of alloying elements in stainless steels has been conducted to eliminate undesirable elements and produce lower activation austenitic (in single phase) stainless steels that have physical properties equivalent to those of the 316SS steel. In order to meet those requirements, the following design conditions have been considered.

(1) Elements of long-life activation, such as Ni, Mo, Nb, Al and Co, were eliminated. Reducing Ni content also leads to a reduction of He production during thermal or mixed spectrum neutron irradiation [6]. Since Ni is the strongest austenite stabilizer, careful adjustment of other elements is required to stabilize the austenite structure without Ni.

(2) Mn is an important element to stabilize the austenite structure. However, an excess amount of Mn accelerates the production of intermetallic compounds and lowers ductility and corrosion resistance. Therefore, Mn was limited between 15% and 35%.

(3) Although C is useful as an austenite stabilizer, it lowers corrosion resistance. Since Ni, which improves corrosion resistance, was not included, C was limited to 0.1%.

(4) N also functions as an austenite stabilizer. But, since it decreases weldability, it was limited to less than 0.2%.

(5) Si is an effective deoxidizing element. An excess amount of Si, however, leads to the destabilization of the austenite structure. As such, the Si content was limited to 1.0%.

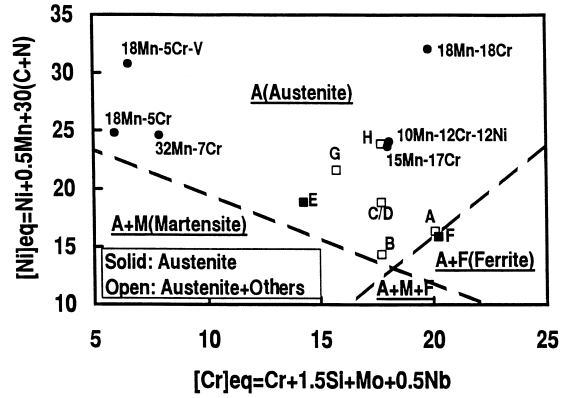

Fig. 1. Prediction of phase constitutions on the Long and DeLong diagram. The proposed alloys and conventional Mn–Cr non-magnetic steels are plotted. The results of the phase constitution of the fabricated alloys are also shown.

(6) A Cr content of more than 12% improves corrosion resistance and increases nitrogen solubility. On the other hand, an excess amount of Cr destabilizes the austenite structure; therefore, the Cr content was limited in the range of 12% to 20%.

(7) Reduction of strength caused by the decreased amounts of C and N can be compensated for by adding V, which is intended to precipitate carbide and/or nitride. However, since an excess of V reduces weldability, V was restricted to 0.3%.

(8) Adjustment of alloying elements was conducted to obtain a single austenitic phase according to the constitution of austenitic stainless steels, which was based on the

Table 1
Designed/evaluated chemical composition and microstructure of the alloys

Alloy ID	Composition	C	Si	Mn	P	S	Ni	Cr	Mo	V	N	Co	Structure
A	Nominal	0.02	0.40	19.5	0.025	0.003	–	19.5	–	–	0.20	< 0.03	γ + X
	Effective	0.021	0.30	19.33	0.027	0.007	0.02	19.43	0.01	< 0.01	0.212	0.002	
B	Nominal	0.02	0.50	15.5	0.025	0.003	–	17.0	–	–	0.20	< 0.03	γ + X
	Effective	0.023	0.47	15.30	0.025	0.007	0.01	16.93	0.01	0.01	0.202	< 0.005	
C	Nominal	0.02	0.50	24.5	0.025	0.003	–	17.0	–	–	0.20	< 0.03	γ + X
	Effective	0.026	0.47	24.67	0.027	0.010	0.01	17.10	0.01	< 0.01	0.209	0.003	
D	Nominal	0.02	0.50	24.5	0.025	0.003	–	17.0	–	0.20	0.20	< 0.03	γ + X
	Effective	0.024	0.48	24.50	0.027	0.006	0.01	17.09	0.01	0.20	0.209	0.002	
E	Nominal	0.02	0.50	24.5	0.025	0.003	–	13.5	–	–	0.20	< 0.03	γ
	Effective	0.025	0.51	24.60	0.025	0.007	0.03	13.40	0.01	< 0.01	0.219	0.003	
F (316SS)	Nominal	0.05	0.50	1.4	0.015	0.003	12.5	17.0	2.5	–	0.04	< 0.03	γ
	Effective	0.059	0.50	1.49	0.017	0.006	12.57	17.49	2.56	< 0.01	0.0432	< 0.01	
G	Nominal	0.02	0.50	30.0	0.025	0.003	–	15.0	–	–	0.20	< 0.03	γ + X
	Effective	0.024	0.46	30.10	0.025	0.009	< 0.01	15.65	< 0.01	< 0.01	0.189	0.002	
H	Nominal	0.02	0.50	34.5	0.025	0.003	–	17.0	–	–	0.20	< 0.03	γ + X
	Effective	0.023	0.53	33.50	0.026	–	–	17.76	–	–	0.190	–	

Chemical compositions were evaluated as wt% from the forged ingot.
Microstructure was observed on the as-rolled plates.
γ: austenite phase, X: Other phases except for γ.

constitution diagrams of Schaeffler [6] and Long and DeLong [14].

Development of the Mn–Cr-based stainless steels was done considering the above factors. Seven types of steels are proposed and their compositions along with that of the conventional 316SS are summarized in Table 1. Alloys A and B are steels based on conventional 18Mn–18Cr and 15Mn–17Cr austenitic stainless steels [15,16], respectively, with reduced C and N contents to improve corrosion resistance and weldability. An additional amount of Mn is added to alloy B to form alloys C and D. Furthermore, V is added to alloy D to compensate for the reduction in strength. For alloy E, the Cr content is reduced in alloy C in order to stabilize the austenite structure. Alloy F is a conventional 316SS, which was used to compare with the newly developed alloys. Alloys G and H contain more Mn and Cr than alloy E.

The proposed alloys were evaluated according to the constitution diagrams of Schaeffler [6] and Long and DeLong [14]. Several Cr and Ni equivalent formulations have been suggested, including the diagram of Long and Delong that has the following formulas (unit: wt%) [14]:

$$[\mathrm{Cr}]\mathrm{eq} = \mathrm{Cr} + 1.5\mathrm{Si} + \mathrm{Mo} + 0.5\mathrm{Nb} \quad (1)$$

$$[\mathrm{Ni}]\mathrm{eq} = \mathrm{Ni} + 0.5\mathrm{Mn} + 30(\mathrm{C} + \mathrm{N}) \quad (2)$$

The calculated values for the proposed alloys are shown in Fig. 1, along with conventional Mn–Cr non-magnetic

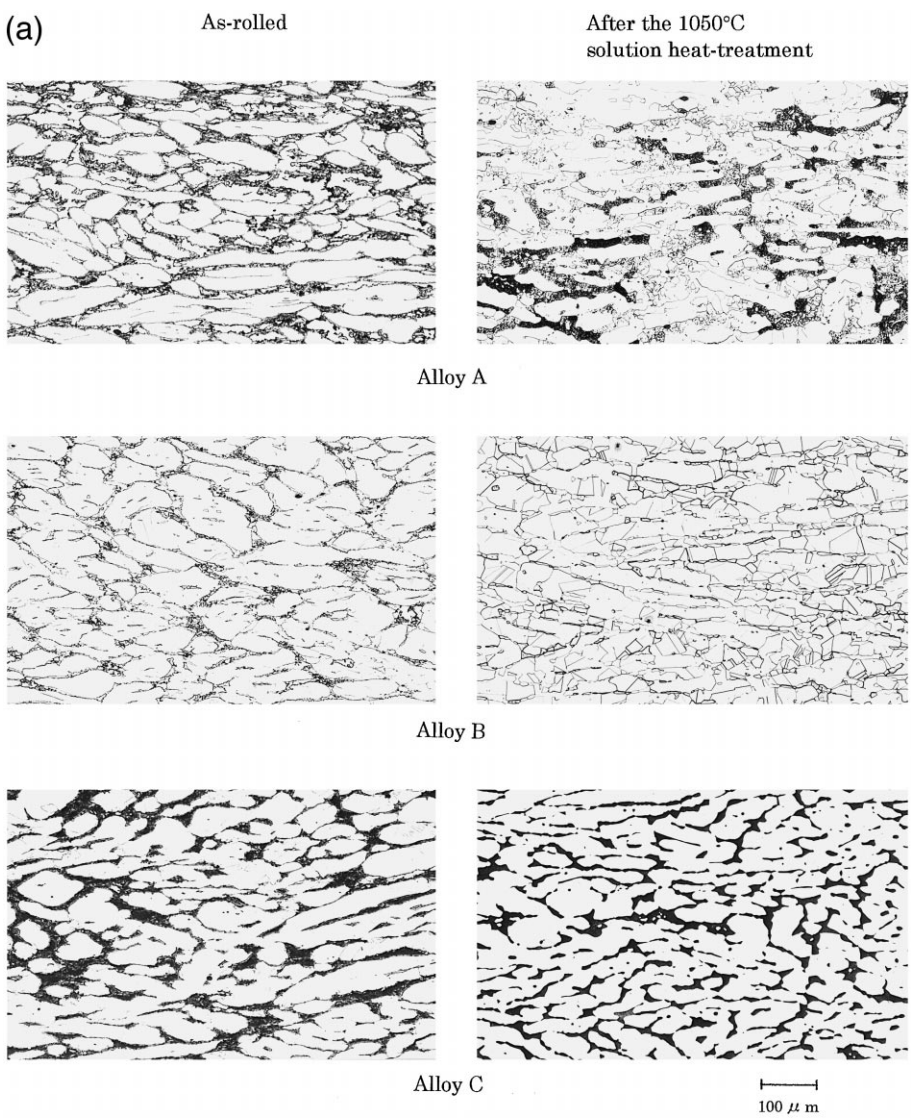

Fig. 2. (a) Microstructures of the fabricated alloys as-rolled and after the 1050°C solution heat-treatment. (b) Microstructures of the fabricated alloys as-rolled and after the 1050°C solution heat-treatment. (c) Microstructures of the fabricated alloys as-rolled.

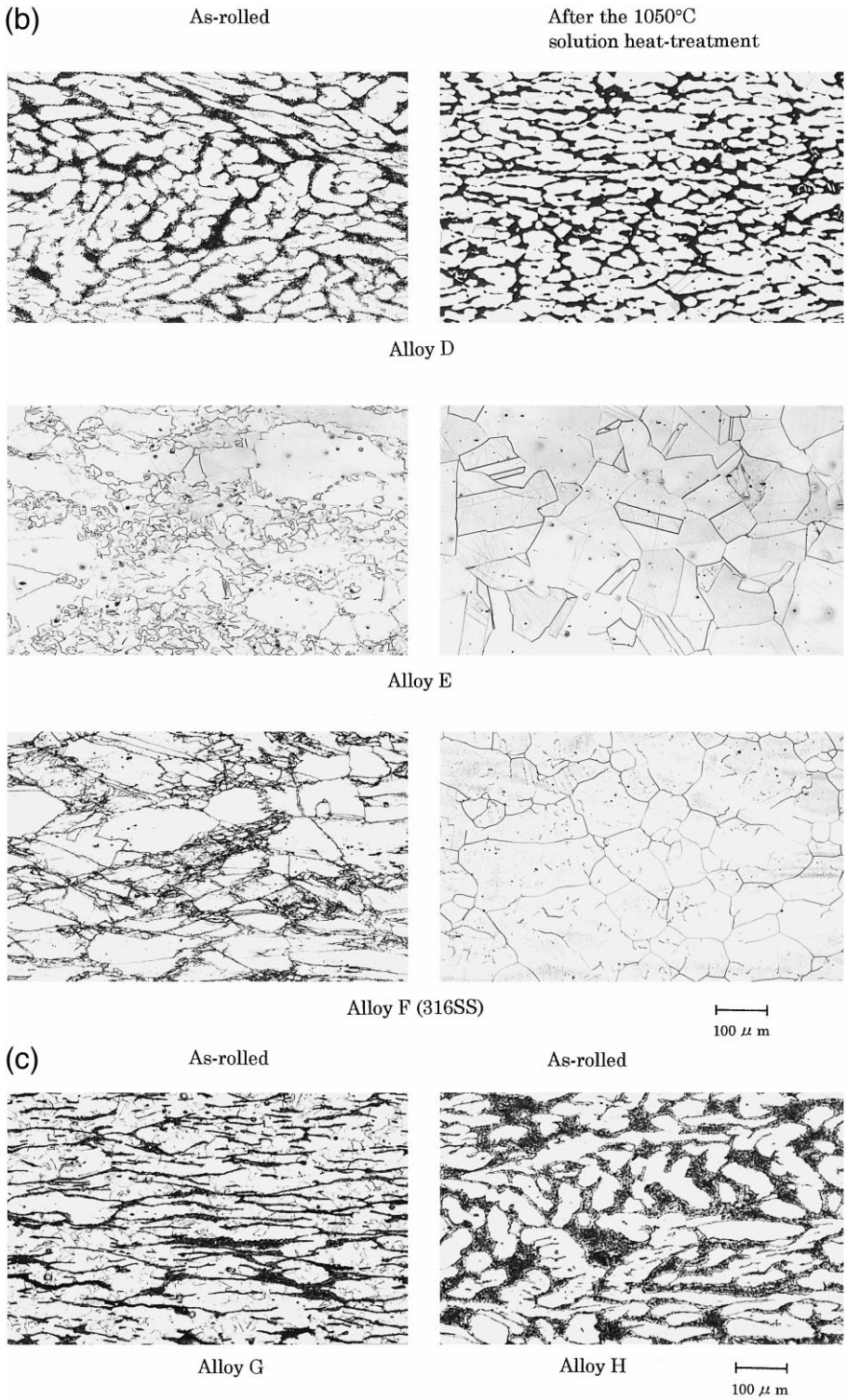

Fig. 2 (continued).

steels. It is expected that the proposed alloys would be fully austenite.

2.2. Preparation of test materials

The eight alloys listed in Table 1 were fabricated. A vacuum high-frequency induction furnace was used to cast a single ingot of about 50 kg (∅ 155 mm × 275 mm) for each alloy. Every ingot was forged to a plate with a 90 mm thickness × 150 mm width × 450 mm length. The forging process was initiated at 1200°C and completed at 800°C. The forged plate was divided into two pieces that were then hot-rolled to a plate with a 30 mm thickness × 150 mm width × 450 mm length. The hot-rolling started at 1180°C and finished at 850°C.

3. Screening tests

Screening tests, such as chemical composition, microstructure, hardness and magnetic permeability, have been conducted on the fabricated alloys to identify those alloys with a single-phase austenite structure. In addition, optimal conditions for solution heat-treatment were evaluated.

The effective chemical compositions of as-rolled plates are also listed in Table 1. The effective compositions are generally in good agreement with the nominal compositions.

The four samples taken from each hot-rolled plate were solution heat-treated at 1010°C, 1050°C, 1090°C and 1130°C for 1 h, respectively, then quenched with cold water. Fig. 2 shows the microstructures of the samples as-rolled and after the 1050°C solution heat-treatment. Examination of the microstructures reveals a single-phase austenite structure for alloys E and F. For alloy A, a duplex structure of grains elongated in the direction parallel to the surface plane was found in the as-rolled and solution heat-treated samples. White contrasted grains in Fig. 2 are austenite grains, while black ones are considered to be mainly intermetallic compounds (such as σ-phase), carbide and δ-ferrite. Alloy B also shows a duplex structure. However, the fraction of the black contrasted grains were found to be less than that in alloy A. The lower contents of Mn and Cr in alloy B compared with alloy A may be the cause. In alloys C, D, G and H, a darker contrast of black grains was observed, showing more intermetallic compounds, etc. This is considered to be due to the higher content of Mn in these alloys as compared to alloy A. Comparing alloys C and D, the addition of V had no significant effect on the micro structure. The reduction of Cr in alloy C to form alloy E is found to be very effective in further stabilizing the austenite structure.

The results of the other screening tests are summarized in Table 2. The strength of alloys A to F was evaluated by hardness testing. The highest Vickers hardness value was obtained for alloy B, which is 215. The data show that the proposed alloys are harder than 316SS (alloy F).

Magnetic permeability and δ-ferrite content were also measured for alloys A to F to examine their magnetic properties. Table 2 shows the results. Ferritic phase was not found in alloys E and F, confirming that they are fully austenite. High permeability and ferrite content were observed in alloys A to D, in agreement with their microstructures. Alloys A to D as-rolled had a lower ferrite content than those which had solution heat-treatment, which is due to the existence of σ-phase in the as-rolled alloys. It is considered that the σ-phase was transformed to δ-ferrite after the solution heat-treatment.

Detailed observation of alloys E and F shows that alloy E had slightly more non-metallic inclusion than alloy F, which may be attributable to the high Mn and N contents. Austenitic grain size [17] was also examined for these two alloys. The results are also presented in Table 2. As the solution temperature increases, the austenitic grain size increases. Although the smallest grain size was found after the solution of 1010°C, recrystallization was insufficient at this temperature. Therefore, the optimal solution temperature is determined to be 1050°C.

4. Evaluation of the developed alloy

The screening tests showed that only alloy E is a suitable candidate for non-magnetic stainless steels. To investigate the applicability of the alloy for reactor structural materials, a wide range of material tests have been conducted, including those for mechanical, thermal and magnetic properties, as well as characteristics of corrosion resistance. In addition, weld joints of the alloy have been evaluated. The material properties of the developed alloy were compared with those of 316SS (alloy F). The samples used were attained with the solution heat-treatment of 1050°C.

4.1. Evaluation of base metal

4.1.1. Physical properties

Tensile properties, i.e., 0.2% yield strength, ultimate tensile strength and elongation, of the alloys were measured at 20°C and 300°C. The results are summarized in Table 3. For both alloys, the tensile and yield strength show an inverse temperature dependence. Both also have similar levels of tensile properties at each temperature.

Table 3 also shows the impact properties of the alloys. The impact values were obtained by a 2 mm V-notch Charpy test at 0°C. Alloy E had a Charpy value of more than 220 J/cm^2, revealing good toughness.

Magnetic permeability was observed on the base metal and the fractured portions of the tensile test and the

Table 2
Results of the screening tests of the alloys

Alloy ID	As-rolled		Solution temperature (°C)															
			1010				1050				1090				1130			
	Mag. per.[a]	Fer. con.[b]	Vick. hard.[c]	Mag. per.[a]	Fer. con.[b]	Aus. grain[d]	Vick. hard.[c]	Mag. per.[a]	Fer.	Aus. grain[d]	Vick. hard.[c]	Mag. per.[a]	Fer. con.[b]	Aus. grain[d]	Vick. hard.[c]	Mag. per.[a]	Fer. con.[b]	Aus. grain[d]
A	> 2	13.2	209	> 2	> 30	–	213	> 2	> 30	–	208	> 2	> 30	–	212	> 2	> 30	–
B	> 2	16.5	210	> 2	> 30	–	209	> 2	28.9	–	214	> 2	> 30	–	215	> 2	> 30	–
C	1.0055	0	196	> 2	> 30	–	196	> 2	> 30	–	192	> 2	> 30	–	197	> 2	> 30	–
D	1.0140	0	201	> 2	> 30	–	199	> 2	> 30	–	203	> 2	> 30	–	199	> 2	> 30	–
E	1.0028	0	182	1.0060	0	3.2	181	1.0050	0	2.5	174	1.0035	0	2.0	157	1.0040	0	1.1
F (316SS)	1.0050	0	140	1.0052	0	4.7	139	1.0058	0	4.1	149	1.0059	0	3.5	136	1.0062	0	3.0

[a] Magnetic permeability.
[b] Ferrite content.
[c] Vickers hardness under the indentation load of 10 kgf.
[d] Austenitic crystal grain size. The grain size number (N) depends on the number of grains per millimeter squared, as defined by $n = 2^{N+3}$ [17].

Table 3
Mechanical properties of the alloys (base metal)

Alloy ID	Vickers hardness	Tensile properties						Charpy impact value (J/cm^2)	Magnetic permeability[a]
		20°C			300°C				
		0.2% Yield (MPa)	Tensile (MPa)	Elongation (%)	0.2% Yield (MPa)	Tensile (MPa)	Elongation (%)		
E	182	315	629	62.9	181	476	43.2	233	1.0050
	181	335	634	61.1	178	477	44.0	225	1.0008
								224	1.0012
F (316SS)	156	253	572	61.5	166	483	43.6	324	1.0058
	139	269	573	62.0	177	485	44.9	330	1.0020
								348	1.0030

Samples were solution heat-treated at 1050°C × 1 h and water quenched.
[a] Upper row = base metal; middle row = fractured portion of tensile test specimens; lower row = fractured portion of Charpy impact test specimens.

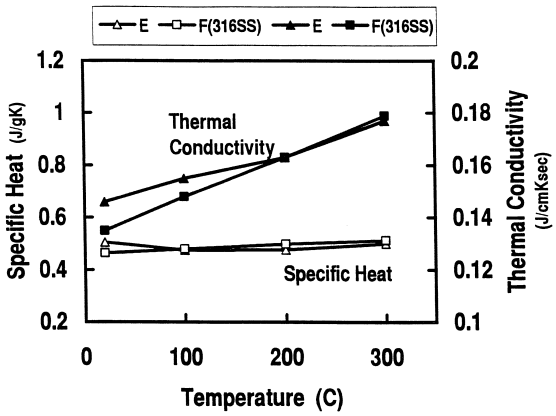

Fig. 3. Temperature dependence of the specific heat and thermal conductivity for the developed 24.5Mn–13.5Cr–0.02C–0.2N alloy (alloy E) and conventional 316SS (alloy F).

Charpy impact test specimens. As shown in Table 3, the permeability of the fractured portions of the test specimens was not influenced by plastic deformation. Conclusively, like 316SS, alloy E has a very stable austenite phase.

The thermal properties of the alloys have been measured. Fig. 3 shows the specific heat and thermal conductivity measured by a laser-flash method as a function of temperature. The results of thermal expansion coefficient as a function of temperature are summarized in Fig. 4. Alloy E has a slightly higher thermal conductivity and a lower thermal expansion coefficient than 316SS.

4.1.2. Corrosion resistance

Various types of corrosion tests have been conducted and the results are summarized in Table 4. A 10% oxalic acid etch test [18] was conducted to observe grain boundaries. Alloy F samples that had a solution heat-treatment had no ditch at the grain boundaries, indicating a good intergranular corrosion resistance. For alloy E, on the other hand, it was seen that some of the grains were surrounded partially by a ditch. After being sensitized at 650°C × 2 h and air cooled, the two alloys developed some grains surrounded by a ditch, indicating a reduction in corrosion resistance.

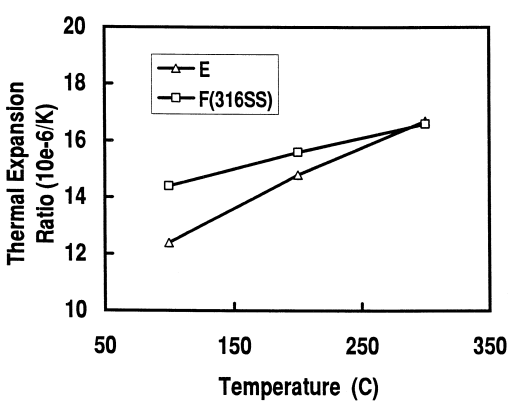

Fig. 4. Temperature dependence of the thermal expansion coefficient for the developed 24.5Mn–13.5Cr–0.02C–0.2N alloy (alloy E) and conventional 316SS (alloy F).

A copper sulfate–sulfuric acid test [19] was also conducted to examine the intergranular corrosion. Similar results as those listed above were obtained. No crack was found at the grain boundaries for the solution-treated samples, while cracks were observed on the sensitized samples.

Corrosion resistance was quantitatively evaluated for both alloys by 5% sulfuric acid testing and ferric chloride testing, which revealed the general corrosion rate and the pitting corrosion rate, respectively [20,21]. Table 4 shows those results. It was shown that alloy E has less corrosion resistance than that of 316SS. This is considered to be due mainly to the higher contents of Cr, Ni and Mo in alloy E.

The above results show that the newly developed alloy has poor resistance against intergranular, general and pitting corrosion relative to that of 316SS. However, it should be noted that the above corrosion tests were conducted under an extremely corrosive environment that does not accurately reflect the actual environment in fusion reactors.

To investigate further the applicability of alloy E for reactors, additional corrosion tests have been performed. Test specimens were exposed to a 19.1% H_3BO_3 water that was pressurized at 0.5 MPa at 80°C for a month in order to simulate actual environmental conditions found in a reactor, which is cooled by H_3BO_3 water. The general and crevice corrosion rates were measured. In addition, susceptibility of the alloy to SCC was examined using a double U-bend test specimen. The results are summarized in Table 4. Alloy E has a corrosion rate as low as that of 316SS. Also, no cracks were observed in the two alloys after SCC tests. Therefore, it can be concluded that, in an actual environment, no significant inferiority in corrosion resistance exists in the developed alloy when compared with 316SS.

4.2. Evaluation of weld joint

The soundness of the weld joint of alloy E has been evaluated using the electron beam (EB) welding method. EB accelerated at 65 kV with a 37 mA current was applied to the 7 mm thick plates of both alloys at a traveling speed of 900 mm/min. Fig. 5 presents the microstructures of the weld joints. No defects, such as cracks and cavities, were found in the weld joints of either alloy.

Tensile properties and Charpy impact value were obtained for the weld joints. The results are shown in Table 5. The 0.2% yield strength of the weld joint for both alloys was slightly increased. The ductility of the weld metal at room temperature was somewhat reduced for alloy F,

Table 4
Corrosion test results of the alloys (base metal)

	Test case	General corrosion tests [18–21]				Tests under actual environment[a]		
		10% oxalic acid etch test	Copper sulfate/ sulfuric acid test	5% sulfuric acid test	Ferric chloride test	General corrosion	Crevice corrosion	Stress corrosion cracking
	Evaluation item	Etch-structure at grain boundary	Damage	Corrosion rate ($g/(m^2\ h)$)	Corrosion rate at 35°C/15°C ($g/(m^2\ h)$)	Corrosion rate ($g/(m^2\ h)$)	Corrosion rate ($g/(m^2\ h)$)	Damage
Alloy E	As SLT[b]	Dual (partial ditch)	No crack	1021.7 1000.9	267.9/181.5	< 0.6 < 0.6	< 1.0 < 1.0	No crack
	Sensitized[c]	Ditch	Crack	1079.5 1021.9	256.5/178.4	–	–	–
Alloy F (316SS)	As SLT[b]	Step (no ditch)	No crack	41.9 42.0	1.36/0.007	< 0.6 < 0.6	< 1.0 < 1.0	No crack
	Sensitized[c]	Ditch	Crack	176.3 200.9	12.7/2.2	–	–	–

[a]After 19.1% H_3BO_3 at 80°C × 1 month.
[b]Samples were solution heat-treated at 1050°C × 1 h and water quenched.
[c]Samples were sensitized at 650°C × 2 h and air cooled.

Table 5
Mechanical properties of the alloys (weld joint)

Alloy ID	Tensile properties								Charpy impact value (J/cm^2)	Magnetic permeability[a]
	20°C				300°C					
	0.2% Yield (MPa)	Tensile (MPa)	Elongation (%)	Location of fracture	0.2% Yield (MPa)	Tensile (Mpa)	Elongation (%)	Location of fracture		
E	358	663	64.3	Base	223	472	44.3	Base	220	1.0030
	350	640	60.7	Base	231	469	39.8	Base	228	1.0055
F (316SS)	307	546	48.6	Base	216	469	41.4	Weld	212	1.0040
	302	553	55.0	Base	221	478	42.9	Base	228	1.0080

Samples were solution heat-treated at 1050°C × 1 h and water quenched, then welded by an electron beam.
[a]Upper row = base metal; lower row = weld metal.

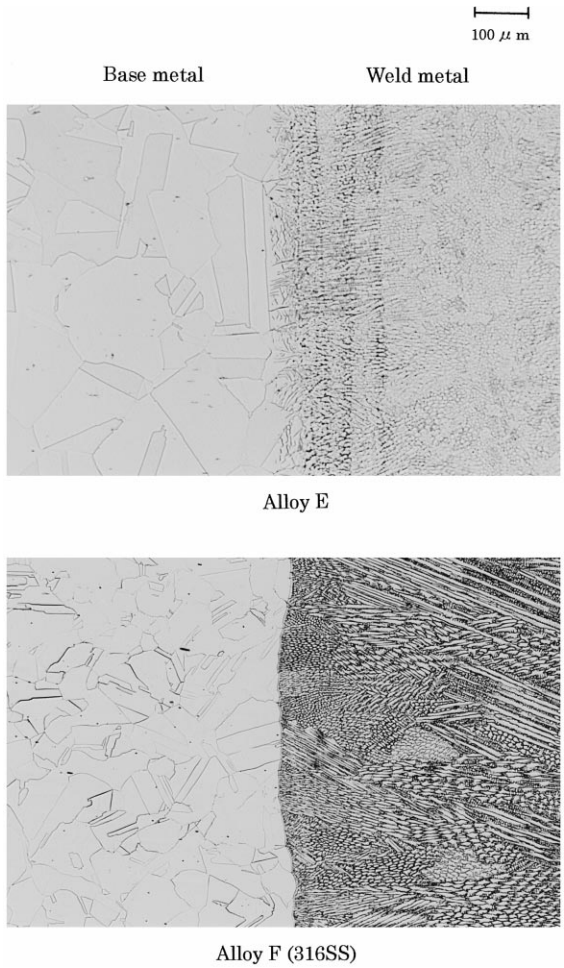

Fig. 5. Microstructures of the weld joints for the developed 24.5Mn–13.5Cr–0.02C–0.2N alloy (alloy E) and conventional 316SS (alloy F).

while that for alloy E stayed at the same level. The Charpy impact values of both alloys exceeded 200 J/cm^2, showing appropriate toughness.

Fig. 6 shows the distribution of the Vickers hardness traversing the weld joints. As in the case of the base metal, alloy E showed a slightly greater hardness value as a weld metal than alloy F. However, the highest Vickers hardness value obtained for alloy E was still about 230, which will not be a serious problem from the points of ductility and toughness as found in the above tests of mechanical properties.

Magnetic permeability was measured for the base metal and weld metal. It was found that the permeability of both alloys slightly increased on the weld metal compared with the base metal. However, the increase in both alloys was insignificant.

The corrosion test using 19.1% H_3BO_3 pressurized water was also applied for a month to the weld joints. It

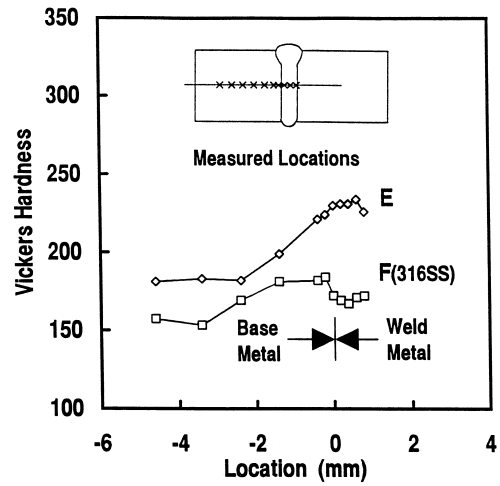

Fig. 6. Distribution of the Vickers hardness traversing the weld joint for the developed 24.5Mn–13.5Cr–0.02C–0.2N alloy (alloy E) and conventional 316SS (alloy F).

was found that both alloys had low corrosion rates for general corrosion [$<$ 0.6 mg/(m^2 h)] and crevice corrosion [$<$ 1.0 mg/(m^2 h)]. Susceptibility of the alloys to SCC was also shown to be negligible.

5. Discussion

Seven types of Mn–Cr-based stainless steels were proposed and expected to be fully austenite. However, the results showed that only alloy E is a single-phase austenitic steel. The stability of the austenite phase has been evaluated generally using the Schaeffler [6] and Long and DeLong [14] constitution diagrams, which show the formation limitations of martensite and ferrite phases by evaluating Ni and Cr equivalents. Since the proposed alloys contain N, the Long and DeLong diagram shown in Fig. 1 was used [14]. However, experimental results showed that the Long and DeLong diagram is not applicable to the proposed alloys with low Ni and high Mn contents. It is considered that the contribution of Mn to γ-phase stability is not as high as that defined by Eq. (2) for high Mn steels. A similar conclusion was also drawn for the Schaeffler diagram.

Hull [22] has developed Ni and Cr equivalents that provide new and modified coefficients for a greater variety of alloying elements. The Ni and Cr equivalents are defined by the following formulas:

$$[\mathrm{Cr}]\mathrm{eq} = \mathrm{Cr} + 1.21\mathrm{Mo} + 0.48\mathrm{Si} + 2.27\mathrm{V} + 0.72\mathrm{W} + 2.20\mathrm{Ti} + 0.14\mathrm{Nb} + 0.21\mathrm{Ta} + 2.48\mathrm{Al}, \quad (3)$$

$$[\mathrm{Ni}]\mathrm{eq} = \mathrm{Ni} + 0.11\mathrm{Mn} - 0.0086\mathrm{Mn}^2 + 0.41\mathrm{Co} + 0.44\mathrm{Cu} + 18.4\mathrm{N} + 24.5\mathrm{C}. \quad (4)$$

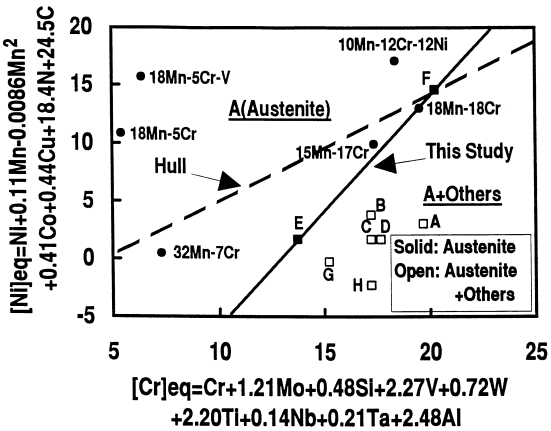

Fig. 7. Prediction of phase constitutions on the Hull diagram. The proposed alloys and conventional Mn–Cr non-magnetic steels are plotted. Results of the phase constitution of the fabricated alloys are also shown.

Fig. 7 shows the calculated values for the studied alloys and conventional Mn–Cr non-magnetic steels. The boundary lines distinguishing the single austenite phase from the other phases are also shown. One of the boundary lines is the line proposed by Hull [22], the other is the one obtained in this study as well as by the results of the conventional 18Mn–18Cr and 15Mn–17Cr austenitic stainless steels [15,16]. The newly obtained boundary line in the Hull diagram would be more applicable for high Mn steels.

6. Conclusion

Seven types of Mn–Cr-based stainless steels were proposed as structural materials for a fusion reactor. Alloying elements of long-life activation, such as Ni, Mo and Co, were eliminated to reduce an induced activation of the alloys. The proposed alloys were expected to be fully austenite according to the Schaeffler and Long and DeLong constitution diagrams. However, the results showed that only one of the seven alloys, 24.5Mn–13.5Cr–0.02C–0.2N (alloy E), was fully austenite. It is considered that the Mn contribution to γ-phase stability is not as high as defined by Schaeffler and Long and DeLong. As such, their diagrams are not applicable for the proposed alloys with low Ni and high Mn contents. For the proposed alloys, Cr and Ni equivalent formulations defined by Hull were found to be more suitable. The boundary line distinguishing the single austenite phase from the others in the Hull diagram has been redefined for the Mn–Cr steels with low C and high N contents.

The developed 24.5Mn–13.5Cr–0.02C–0.2N alloy showed excellent tensile, hardness, thermal and magnetic properties comparable or superior to those of 316SS. Its austenite structure was sufficiently stable so as not to be influenced by plastic deformation. Although the Charpy impact value was found to be lower than that of 316SS, it was still within an acceptable range. Under an extremely corrosive environment, the developed alloy showed poor resistance against intergranular, general and pitting corrosion relative to that of 316SS. However, under H_3BO_3 water simulating the actual environment of a fusion reactor, no crucial inferiority in corrosion resistance was found when compared with 316SS. The SCC resistance of the alloy was also equivalent to that of 316SS. Weldability of the alloy was also similar to that of 316SS. In addition, no significant decrease in its mechanical properties, magnetic permeability and corrosion resistance was found for the weld joints, compared with those of 316SS. The developed alloy can be manufactured along usual production lines.

To confirm the applicability of the newly developed Mn–Cr alloy for a fusion reactor, further investigation will be required, including the investigation of the neutron irradiation effects on the alloy. In addition, finer adjustment of the alloying elements could further reduce the radioactivity and improve the physical properties and corrosion resistance, etc.

References

[1] E.E. Bloom, R.W. Conn, J.W. Davis, R.E. Gold, R. Little, K.R. Schultz, D.L. Smith, F.W. Wiffen, J. Nucl. Mater. 122&123 (1984) 17.
[2] R.W. Conn, E.E. Bloom, J.W. Davis, R.E. Gold, R. Little, K.R. Schultz, D.L. Smith, F.W. Wiffen, Nucl. Technol./Fusion 5 (1984) 291.
[3] P. Fenici, D. Boerman, V. Coen, E. Lang, C. Ponti, W. Schule, Nucl. Eng. Des./Fusion 1 (1984) 167.
[4] G. Piatti, S. Matteazzi, G. Petrone, Nucl. Eng. Des./Fusion 2 (1985) 391.
[5] G. Piatti, P. Schiller, J. Nucl. Mater. 141–143 (1986) 417.
[6] G. Piatti, D. Boerman, J. Heritier, Development of low activation Cr–Mn austenitic steels for fusion reactor applications, Proceedings of the 15th Symposium on Fusion Technology, 1988, pp. 983–990.
[7] M. Zucchetti, M. Zublena, A study on the prospects for development of a new low activity austenitic stainless steel for fusion applications, Proceedings of the 15th Symposium on Fusion Technology, 1988, pp. 991–996.
[8] M. Merola, M. Zucchetti, Comparison of thermal behaviour and activation of some proposed materials for fusion reactor first wall, Proceedings of the 16th Symposium on Fusion Technology, 1990, pp. 327–330.
[9] D.R. Harries, G.J. Butterworth, A. Hishinuma, F.W. Wiffen, J. Nucl. Mater. 191–194 (1992) 92.
[10] A. Kohyama, M.L. Grossbeck, G. Piatti, J. Nucl. Mater. 191–194 (1992) 37.
[11] V.K. Shamardin, T.M. Bulanova, V.S. Neustroyev, Z.E. Ostrovsky, V.M. Kosenkov, L.I. Ivanov, E.V. Djomina, J. Nucl. Mater. 191–194 (1992) 706.

[12] V.K. Shamardin, T.M. Bulanova, V.N. Golovanov, V.S. Neustroyev, A.V. Povstyanko, Z.E. Ostrovsky, J. Nucl. Mater. 233–237 (1996) 162.
[13] H. Takahashi, S. Ohnuki, H. Kinoshita, S. Nakahigashi, J. Nucl. Mater. 179–181 (1991) 629.
[14] C. Long, W. DeLong, Welding J. 52 (7) (1973) 281s, Welding research supplement.
[15] K. Orita, Y. Ikeda, T. Iwadate, J. Ishizaka, ISIJ Int. 30 (8) (1990) 587.
[16] K. Ohnishi, R. Miura, H. Tsukada, K. Sekimura, H. Moritani, A. Fuji, JSW Tech. Rev. 40 (1981) 12 (in Japanese).
[17] Japan Standards Association, Method of austenitic grain size test for steel, Japan Industrial Standard G0551 (in Japanese), 1997.
[18] Japan Standards Association, Method of 10% oxalic acid etch test for stainless steels, Japan Industrial Standard G0571 (in Japanese), 1980.
[19] Japan Standards Association, Method of copper sulfate–sulfuric acid test for stainless steels, Japan Industrial Standard G0575 (in Japanese), 1980.
[20] Japan Standards Association, Method of 5% sulfuric acid test for stainless steels, Japan Industrial Standard G0591 (in Japanese), 1980.
[21] Japan Standards Association, Method of ferric chloride test for stainless steels, Japan Industrial Standard G0578 (in Japanese), 1981.
[22] F.C. Hull, Welding J. 52 (5) (1973) 193s, Welding research supplement.